Niobium-Doped Titania Nanoparticles: Synthesis and Assembly into Mesoporous Films and Electrical Conductivity

Yujing Liu,[†] Johann M. Szeifert,[†] Johann M. Feckl,[†] Benjamin Mandlmeier,[†] Jiri Rathousky,[‡] Oliver Hayden,[§] Dina Fattakhova-Rohlfing,[†,*] and Thomas Bein[†,*]

[†]Department of Chemistry and Center for NanoScience (CeNS), University of Munich (LMU), Butenandtstrasse 5-13, 81377 Munich, Germany, [‡]J. Heyrovský Institute of Physical Chemistry, v.v.i., Academy of Sciences of the Czech Republic, Dolejskova 3, 18223 Prague 8, Czech Republic, and [§]Siemens AG, Corporate Technology, CT T DE HW3, Guenther-Scharowsky-Str. 1, 91050 Erlangen, Germany

ABSTRACT Crystalline niobium-doped titania nanoparticles were synthesized *via* solvothermal procedures using *tert*-butyl alcohol as a novel reaction medium, and their assembly into mesoporous films was investigated. The solvothermal procedure enables the preparation of crystalline doped and undoped nonagglomerated titania nanoparticles, whose size can be controlled from 4 to 15 nm by changing the reaction temperature and time. The anatase lattice of these particles can incorporate more than 20 mol % of Nb ions. The nanoparticles can be easily dispersed at high concentrations in THF to form stable colloidal suspensions and can be assembled into uniform porous mesostructures directed by the commercial Pluronic block copolymer F127. The resulting mesoporous films show a regular mesostructure with a d spacing of about 17 nm, a uniform pore size of about 10 nm with crystalline walls, a high porosity of 43%, and a large surface area of 190 $m^2 cm^{-3}$. Substitutional doping with niobium ions drastically increases the electrical conductivity of the titania particles. The electrical conductivity of as-prepared nanoparticles containing 20 mol % of Nb is 2×10^{-5} S cm^{-1}; it increases to 0.25 S cm^{-1} after treatment at 600 °C in nitrogen.

KEYWORDS: nanoparticle synthesis · nanoparticle self-assembly · conducting transparent oxides · mesoporous films · titania

Transparent conducting oxides (TCOs) with a regular mesoporous architecture have recently attracted attention owing to their ability to accommodate functional guest molecules in photovoltaic, electrochromic, and chemical sensing applications, where the access of both photons and charge carriers to a large interface is of key importance.[1−3] However, the range of compounds that simultaneously feature electrical conductivity and optical transparency in the visible spectrum is limited.[4] TCOs usually consist of doped indium, tin, zinc, or cadmium oxides; of these, only tin-doped indium oxide (ITO) and antimony-doped tin oxide (ATO) have been prepared with a periodic porous morphology.[1−3,5] The synthesis of mesoporous electrodes from other classes of TCOs is of great interest, as it could substantially extend the library of available transparent conducting nanoarchitectures meeting the requirements of different optoelectronic applications.

In 2005, Furubayashi *et al.*[6,7] reported a metallic type conductivity of Nb-doped anatase titania (NTO) films. Thin films, epitaxially grown by pulsed laser deposition, exhibit a conductivity of $10^3−10^4$ S cm^{-1} and high optical transmittance in visible light, which makes them comparable with the much more expensive ITO. The conductivity mechanism was explained by the formation of an impurity band overlapping with the conduction band of anatase and corroborated by first-principles band calculations showing that Nb doping does not change band dispersions except for filling the conduction band, implying that Nb atoms do not generate in-gap states.[8]

The idea to synthesize mesoporous transparent titania-based electrodes is appealing, as titania films with controlled mesoporous structure can be easily prepared. An increase in electrical conductivity of the existing mesostructures due to doping with Nb atoms could open a way to inexpensive nanostructured TCO materials with controlled porosity. Moreover, the already known applications of titania, such as in photovoltaics, photocatalysis, and charge storage, could greatly benefit from an increased electrical conductivity of the titania framework. This has recently been demonstrated by Huang *et al.*, who reported that higher conductivity of a TiO_2 electrode by Nb doping leads to enhanced photovoltaic performance.[9]

Fabrication of periodic mesoporous Nb-doped titania films has been reported by Sanchez et al.[10] and Wu et al.;[14] however, the electrical conductivity of those materials was not investigated. Disordered porous NTO powders[11,13,15] and films[12] have also been reported, but these materials were studied regarding their photocatalytic and electrocatalytic behavior. Additional studies dealing with the preparation of conducting titania materials usually involve physical processes or high-temperature solid-state reactions, which are not conducive for the fabrication of periodic porous nanostructures.[16−29]

Periodic mesoporous titania films with controlled porous structure can be prepared by the self-assembly of amorphous titania sols, crystalline nanoparticles, or a combination of both in the presence of surfactants acting as structure-directing agents.[9,30−32] It was recently demonstrated for mesoporous thin films of antimony-doped tin oxide (ATO) that TCO nanocrystals can also serve as building blocks for the assembly of nanostructured transparent electrodes.[33] The doping level and thus the electrical conductivity can be precisely adjusted because their composition can be controlled in the particle synthesis. Due to the intrinsic crystallinity of the building blocks, crystalline mesostructures can be obtained already at moderate temperatures. However, the use of nanoparticles as the primary units for the assembly of mesoporous conducting films implies certain requirements regarding their properties. The particles should be just a few nanometer in size with a narrow particle size distribution, feature crystallinity and electrical conductivity, and should be dispersible in various solvents to form stable colloidal solutions. The synthesis of Nb-doped titania nanoparticles meeting those criteria has not been reported so far. Recently, we have reported that *tert*-butyl alcohol can be used as a novel reaction medium for the solvothermal synthesis of ultrasmall and highly dispersible nanoparticles.[34] The use of *tert*-butyl alcohol in microwave-assisted synthesis provides monodispersed nanosized particles of titania, whose size and crystallinity can be easily controlled by the variation of reaction temperature and time.

Here we describe the solvothermal synthesis of crystalline monodispersed niobium-doped titania nanoparticles using *tert*-butyl alcohol as a novel reaction medium and an oxide source. Furthermore, the ability of the obtained nanocrystals to self-assemble into complex 3D mesoporous nanostructures and the electrical conductivity of the nanoparticles and mesoporous films are investigated.

RESULTS

Synthesis of Nb-Doped TiO$_2$ Nanoparticles and Their Assembly into Mesoporous Films.
For the preparation of niobium-doped titania nanoparticles, titanium tetrachloride and niobium(V) ethoxide were dissolved in *tert*-butyl alco-
hol. The particles with different Nb content are designated as NPX, where X is the Nb/(Nb + Ti) molar ratio in percent. The clear solution was kept at different temperatures and different times in a laboratory oven in a Teflon-sealed autoclave. The solution turned turbid when the nanoparticle formation started. The particle size and crystallinity strongly depend on the reaction temperature. At 60 °C, the particles are still completely amorphous, and an increase in the reaction temperature to 100 °C is necessary to obtain a crystalline phase (Figure S1, Supporting Information). A further increase in the reaction temperature leads to larger crystalline particles. Thus, the size of the NP20 particles obtained after 12 h of reaction at 100 and 150 °C is 10 and 14 nm, respectively.

An increase in the concentration of Nb leads to a delayed formation of particles. For the particles prepared at 100 °C, the onset of crystallization was observed (by XRD) after 1.5, 3, and 4 h for NP0, NP10, and NP20, respectively. This effect, also reported for other synthesis procedures,[35,13,15] is attributed to the suppression of particle crystallization due to Nb doping. Furthermore, the particle size at the same reaction temperature can be varied by changing the reaction time. While NP20 particles synthesized at 100 °C for 4 h are only 4 nm in size, prolonging the reaction time to 20 h increases the particle size to 13 nm (Figure 1b).

As we aimed at the preparation of crystalline nanoparticles as small as possible, the reaction at 100 °C was stopped just after the onset of crystallization. The NTO nanoparticles with different Nb content prepared this way are crystalline and average 4−5 nm in size (Table S1 in Supporting Information), as shown by XRD patterns (Figure 1a) and HRTEM images (Figure 2). The XRD patterns of both pure and doped nanoparticles with up to 20 mol % of niobium show only one crystalline phase, either anatase or a phase structurally closely related to anatase (Figure 1a). An increase in the Nb content leads to a shift of the (101) and (200) reflections to lower angles corresponding to the unit cell expansion of about 5% due to the replacement of Ti^{4+} ions (radius 60.5 pm) by slightly larger Nb^{5+} ions (radius 64 pm) according to Vegard's law. The same changes in *d* spacing with increasing Nb content were observed in the HR-TEM images of doped particles.

All of the nanoparticles can be dispersed easily in tetrahydrofuran (THF) at concentrations of more than 5 wt % of NTO in the presence of small amounts of hydrochloric acid, forming stable transparent colloidal dispersions. The particle size distributions obtained by DLS (Figure 2c) are in good agreement with those obtained from X-ray diffractograms.

To sum up, the undoped as well as Nb-doped titania nanoparticles prepared by the solvothermal synthesis in *tert*-butyl alcohol are crystalline, nanosized, and dispersible, which makes them suitable building blocks
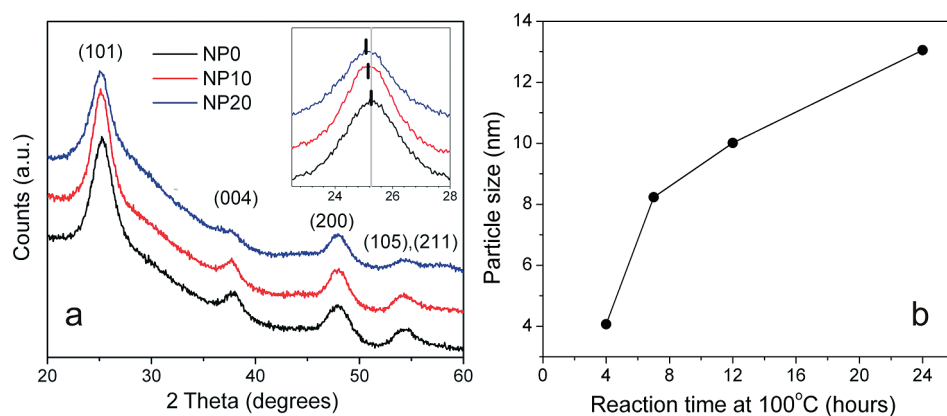
Figure 1. (a) XRD patterns of as-prepared 0, 10, and 20% Nb-doped TiO$_2$ nanoparticles synthesized by a solvothermal reaction in *tert*-butyl alcohol at 100 °C for 1.5, 3, and 4 h, respectively. The inset shows the position of the (101) peak. (b) Variation of the size of NP20 nanoparticles during synthesis in *tert*-BuOH at 100 °C with the reaction time. The particle size was derived from the peak broadening in the XRD patterns according to the Debye−Scherrer equation.

for nanostructured materials assembly. We have examined the applicability of the as-synthesized nanoparticles for the assembly of mesoporous films using the commercial Pluronic F127 polymer as a structure-directing agent. Thin films designated as MS0, MS10, and MS20 were prepared from NP0, NP10, and NP20 nanoparticles, respectively. The synthesis times for the different samples were chosen such that the particle size of all samples was about 4 nm, in order to make the particles compatible with the surfactant-assisted self-assembly. In order to remove the template and to sinter the nanoparticles, the films were heated in air at 300 °C for 2 h because this is the lowest temperature sufficient for the removal of the Pluronic copolymer and the complete removal of organic residues from the interior of the pores in the thin films.[32−34]

The SEM images (Figure 3) show the surface of the mesoporous structures assembled from nanoparticles with varying Nb content. Depending on the composition of the nanoparticles used, the character of the mesostructure of the films differs significantly. The assembly of the undoped NP0 nanoparticles gives a worm-like open mesostructure with a homogeneous pore distribution. The films assembled from NP10 nanoparticles feature a channel-type mesostructure similar to that assembled from antimony-doped tin oxide nanoparti-

cles.[33] Finally, the NP20 particles lead to films with a higher degree of pore ordering, resembling a cubic mesostructure with a *d* spacing of about 17 nm. The thickness of the films assembled from particles with different doping levels is around 200 nm.

The highly porous morphology of the films assembled from nanoparticles is also apparent in TEM images (Figure 4 and Figure S2 in Supporting Information). The Fourier transforms of the TEM images show a ring corresponding to a mesostructure dimension of 16 ± 1 nm. Similar information about the mesostructure ordering is provided by the small-angle XRD patterns (Figure S3, Supporting Information), which exhibit a clearly distinguishable reflection for the MS10 and MS20 samples and a broad shoulder for a less ordered MS0 film. The HRTEM images show that the pore walls are composed of crystalline nanoparticles (Figure 4b,d). The high crystallinity of the films calcined at 300 °C was also proven by wide-angle X-ray diffraction (Figure S4, Supporting Information). The crystalline domain size calculated from the (101) reflection of the corresponding XRD patterns is about 7.5 and 6.5 nm for MS0 and MS20 films, respectively. This illustrates that the crystal size increases after calcination at 300 °C compared to the size of nanoparticles used for the films' assembly.
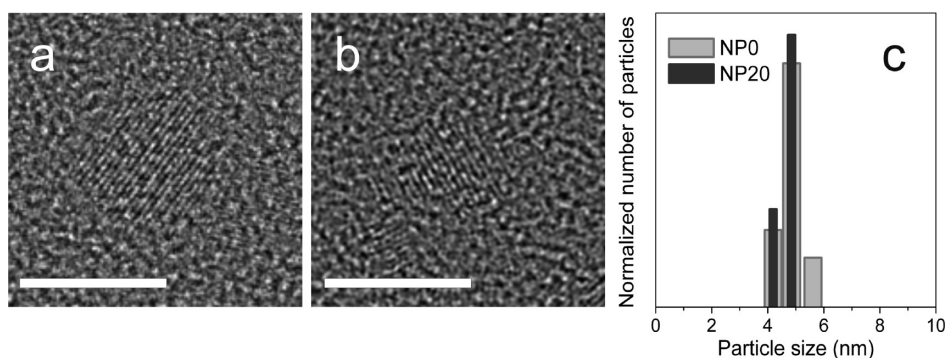

Figure 2. HRTEM images of as-made NP0 (a) and NP20 (b) nanoparticles synthesized at 100 °C (scale bar corresponds to 5 nm), and the particle size distribution of dispersions in tetrahydrofuran determined by DLS (c).
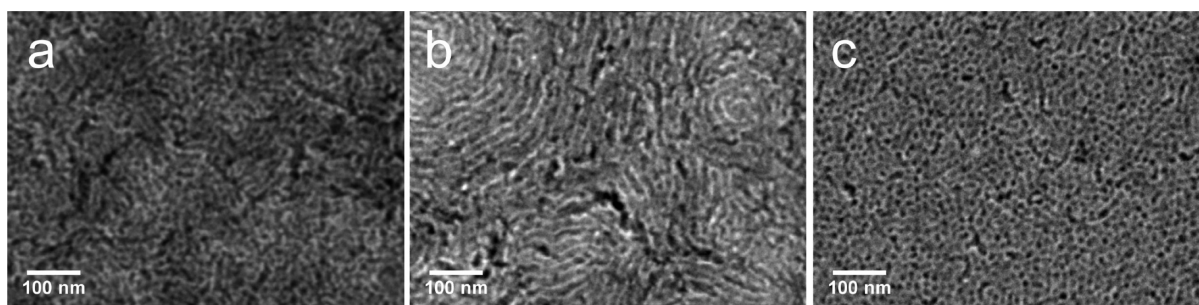
Figure 3. SEM images (top view) of MS0 (a), MS10 (b), and MS20 (c) films calcined in air at 300 °C.

The textural properties and the accessibility of the internal surface of the thin films were studied by krypton adsorption at −196 °C (Figure 5). The samples assembled from nanoparticles are characterized by an open porous structure without pore blocking. The use of particles with a higher Nb content leads to films exhibiting a larger pore volume and surface area, in combination with a higher degree of uniformity of the mesostructure as could be seen in electron microscopy. The MS20 films feature the largest pore volume and a porosity of 43%, with a surface area of 190 $m^2 cm^{-3}$. The pore size determined from the Kr isotherm is 9−10 nm with a narrow pore size distribution, as evidenced by the very steep adsorption and desorption branches. The isotherms of samples MS10 and MS0 are flatter, their pore size distribution is broader, and the surface area is smaller (163 and 90 $m^2 cm^{-3}$, respectively).

Electrical Conductivity of Nb-Doped TiO$_2$ Nanoparticles. The valence state of the metal atoms in the Nb-doped titania lattice is an important indication of successful doping with regard to the electric conductivity, which is directly related to the specific defects formed in the doping process.[36] The valence states of Ti and Nb in the nanoparticles containing 20% of Nb prepared in *tert*-BuOH at 100 °C were investigated using X-ray photoelectron spectroscopy (XPS) (Figure 6), which shows the peaks corresponding to titanium and niobium. About 20 mol % of both titanium and niobium is found in their reduced states, Ti^{3+} and Nb^{4+} or lower,[15] respectively, which is consistent with the Nb doping level of 20%. In case of effective doping by Nb, donor level electrons can reside in the form of reduced valence states of Ti or Nb. From the observation of such states in XPS, we can assume that the extra electrons
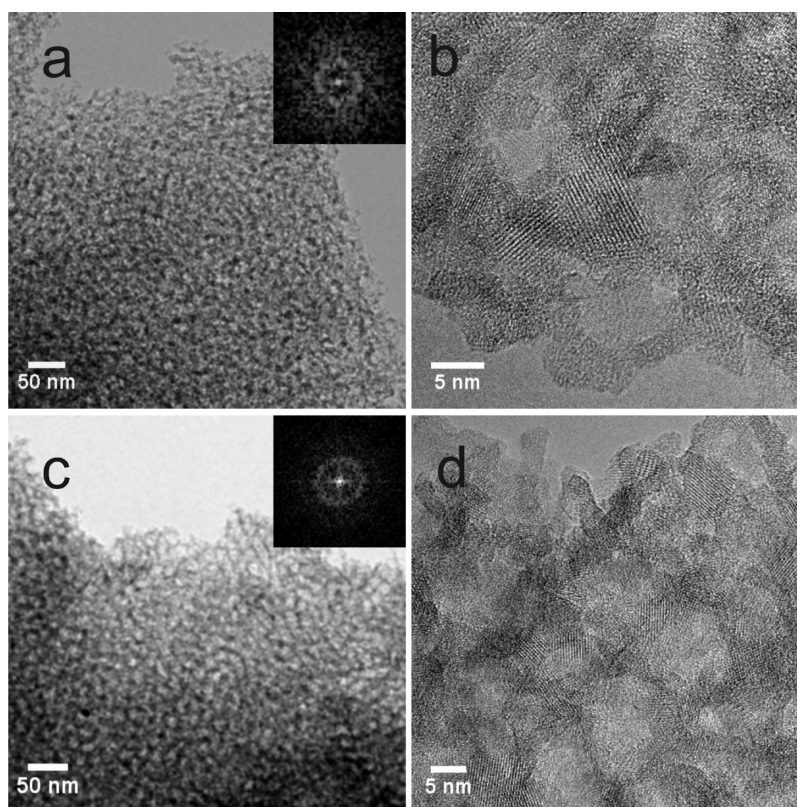

Figure 4. (a,c) TEM and (b,d) HRTEM images of MS10 (first row) and MS20 (second row) samples calcined at 300 °C. The insets in (a,c) show the Fourier transforms of the images.
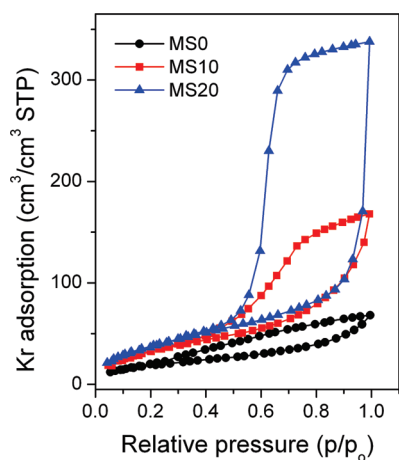
Figure 5. Kr adsorption isotherms at −196 °C of templated mesoporous films assembled from nanoparticles with different Nb content: MS0 (black circles), MS10 (red squares), and MS20 (blue triangles). All of the films were calcined at 300 °C.

Figure 6. XPS spectra of as-prepared NP20 nanoparticles synthesized in *tert*-BuOH at 100 °C. The peaks were assigned according to refs 26 and 37−39.

are not compensated by other defects. Therefore, the introduction of Nb^{5+} ions into the titania lattice leads to the donation of electrons into the conduction band and thus an increase in the charge carrier concentration. The presence of the reduced species due to the Nb doping is also reflected in the particle color. Pressed into a pellet, the as-prepared Nb-doped nanoparticles are bluish-green, the color being more intense for the larger particles, while the undoped TiO_2 particles remain white.

In spite of the presence of Ti in the reduced state, the room temperature electrical dc conductivity (for details, see Supporting Information) of the crystalline nanoparticles prepared at 100 °C is still quite low, *ca.* 1 × 10^{-6} S cm^{-1} for undoped and 2 × 10^{-5} S cm^{-1} for the 20% doped nanoparticles, which is comparable with the data reported by Huang *et al.*[9] for the pressed NTO nanoparticles prepared by hydrothermal synthesis. This could be due to a strong localization of the free electrons and their low mobility. To further improve the electrical conductivity, the as-produced NTO nanoparticles have to be heated in non-oxidizing atmosphere such as nitrogen at 400−600 °C (Figure 7, and Table S2 in Supporting Information). Heating in air leads to an irreversible loss of conductivity, which was also indicated by the change in the particle color to deep-blue or white after heating in N_2 or air, respectively. The change in the conductivity with the Nb content was found to be nonlinear. The introduction of Nb in the anatase lattice drastically increases the conductivity by several orders of magnitude, the highest conductivity being found for the 20% Nb sample, for which the conductivity and the carrier concentration obtained from Hall effect measurements were 0.25 S cm^{-1} and 10^{20} cm^{-3}, respectively. A further increase in the Nb content does not lead to further improvement. The maximum conductivity was obtained for a much higher Nb concentration than for materials prepared by physical
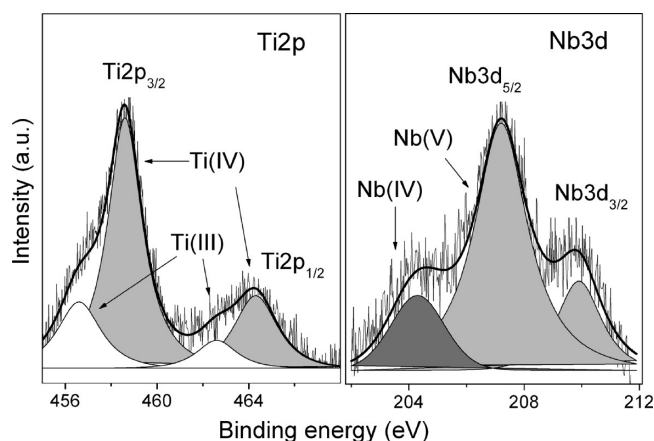
methods, for which the highest conductivity is observed already at 3% of Nb.[40]

An XPS depth profile analysis performed after polishing the particles with argon ions for different time periods reveals that the surface composition of the particles after heating in N_2 at 600 °C differs from that of the bulk. As the niobium content reaches 30.0% at the surface and 19.8% in the bulk, respectively, the particle surface is enriched with niobium. At the surface, both titanium and niobium are in their highest oxidization states (Figure S5, Supporting Information). On the contrary, in the particle core, a part of the titanium atoms is also present as Ti^{3+} cations, their fraction (16%) being similar to the amount of Nb^{5+} cations introduced in the synthesis (about 20%). This indicates that most of the extra electrons generated by Nb doping are released into the conduction band of TiO_2, leading to the formation of Ti^{3+} and resulting in the high conductivity.[8]

The electrical conductivity of mesoporous thin films assembled from different types of nanoparticles is much lower than that of the heated particles and shows much smaller variation with the Nb content. Thus, the conductivity of the doped MS20 films (10^{-4} S cm^{-1}) is
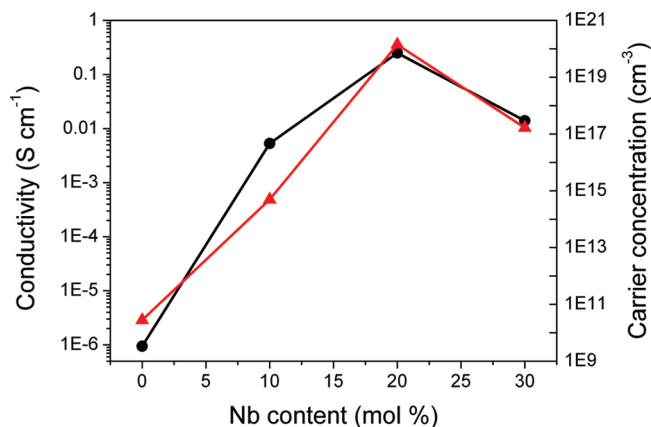

Figure 7. Specific conductivity (black circles) and charge carrier concentration (red triangles) of the pellets pressed from Nb-doped nanoparticles and heated at 600 °C in N_2, as a function of Nb content. The axes are shown in semi-logarithmic scale.

only about two times larger than that of the pure titania film (Table S3, Supporting Information).

DISCUSSION

The results above show that *tert*-butyl alcohol is a suitable reaction medium for the fabrication of crystalline monodispersed nanoparticles. The reaction in *tert*-butyl alcohol can be carried out using microwave heating, as described in our previous publication,[34] and solvothermally at mild temperatures, leading to highly dispersible nanoparticles. The size of the particles and their degree of crystallinity can be controlled by reaction temperature and reaction time, thus enabling the preparation of particles 4−15 nm in size. Besides the pristine oxides, the solvothermal reaction in *tert*-butyl alcohol is suitable for the preparation of doped nanoparticles with homogeneously distributed dopant within the host lattice (before heat treatment, as the latter can lead to surface enrichment, as was shown above by the XPS data). Following this synthesis route, the anatase lattice can incorporate more than 20% of Nb ions. The incorporation of the guest impurities slows down the crystallization rate and leads to some expansion of the anatase lattice.

In contrast to the titania particles prepared by the well-established solvothermal synthesis in benzyl alcohol,[41] the particles of similar size and crystallinity synthesized in *tert*-butyl alcohol can be easily dispersed up to high concentrations in THF to form stable colloidal dispersions. This can be attributed to their different surface chemistry. The different surface properties of nanoparticles synthesized either in aromatic or aliphatic alcohols are the reason for their different ability to self-organize into uniform mesoscopic structures directed by the block copolymers of the polyalkylene oxide type. The particles prepared using *tert*-butyl alcohol assemble into regular mesostructures directed by the Pluronic templates, while those obtained using benzyl alcohol provide only disordered structures with these templates.[32] The films assembled from doped titania nanoparticles exhibit a higher degree of mesostructure ordering than those prepared from undoped ones, which may be due to the different surface properties of nanoparticles with varying Nb content. A similar behavior was observed for the ATO nanoparticle system.[2,33] Generally, the assembly of mesoporous films from particles has a beneficial effect on the porosity in comparison with sol−gel films, especially regarding the open nature of the porous system and as a result the better accessibility of the inner surface.[32] Doping with niobium leads to an enhancement of the mesostructure uniformity, the surface area, and the pore volume.

The incorporation of Nb drastically increases the electrical conductivity of the nanoparticles. The maximum conductivity at room temperature of the 20% Nb-doped sample, reaching 0.25 S cm^{-1}, is remarkably high for the wide band gap semiconductor titania. It supports the assumption that a considerable increase in the electrical conductivity of the anatase lattice is possible due to extrinsic doping with niobium ions. The only other study published to date on the chemical preparation of conducting Nb-doped titania nanoparticles by Huang *et al.*[9] gives similar values of conductivity of as-produced nanoparticles and thus an additional support to the suitability of chemical routes for the preparation of conducting titania particles. Their conductivity is, however, still much lower than the range of 10^3-10^4 S cm^{-1} reported by Furubayashi *et al.*[6,8,17] for epitaxially grown NTO films. It appears to be a general feature of the polycrystalline TCO systems prepared by chemical methods[1,33] that their dc conductivity is lower than the conductivity of analogous materials prepared by physical deposition techniques such as evaporation or magnetron sputtering. This difference is attributed primarily to grain boundary scattering in the polycrystalline material and the larger amount of defects and imperfections in the nanosized crystals. Moreover, for the Nb-doped titania, the situation is even more complicated due to the specific properties of this system. In contrast to the conventionally used indium or tin oxides, which can form solid solutions with various dopants causing only limited distortion of the host crystalline lattice,[4] incorporation of Nb into the anatase lattice can cause a noticeable lattice expansion or lattice deformation reported also by other authors,[39] which generally leads to the decreased electron mobility.[4] Moreover, donated electrons are susceptible to compensation by easily formed defects, such as Ti vacancies or oxygen interstitials.[26,42]

Further improvement of the electrical conductivity requires an optimization of the reaction conditions. It appears that at least two factors are important for obtaining a highly conductive niobium-doped titania semiconductor. First, doped Nb atoms must be homogeneously distributed within the anatase lattice. Second, the formation of other defects except for the replacement of tetravalent Ti with pentavalent Nb should be avoided, as the extra electrons caused by Nb doping and existing in the form of Ti^{3+} and/or Nb^{4+} are easily compensated by titanium vacancies or oxygen interstitials. The conductivity of the as-prepared nanoparticles is rather low and can be substantially increased by a treatment at elevated temperatures in non-oxidizing atmosphere. The reasons that can contribute to the greatly enhanced conductivity of the pressed particle pellets after thermal treatment are particle growth, particle sintering, and pyrolysis of the organic residues acting as an insulator. However, such a treatment can lead to the undesired partial surface segregation of Nb due to a "self-purification" process described for NTO as well as for other doped oxides due to the size mismatch of the metal cations.[26,43,44]

The mesoporous layers assembled from the Nb-doped titania nanoparticles show very good structural

properties such as the order of the porous system, a uniform pore size, a high pore volume, a large surface area, and crystallinity of the walls. However, the increase in conductivity due to Nb doping is much less pronounced for the mesoporous films than for the similarly treated particles. We tentatively attribute this (i) to the much smaller size of the crystals in the walls of the mesoporous films compared to that of the pressed pellets after heating (7 and 22 nm, respectively) due to the confining effect of the template, and (ii) the oxidation of a surface layer by adsorbed oxygen molecules upon exposure to air due to the high surface area of the films.

Now that the concept has been proven to be successful for making uniform porous conducting architectures on the basis of Nb-doped titania, future efforts should be aimed at the improvement of the conductivity of the mesoporous films. One of the ways to increase the conductivity can be the use of the bigger crystals for the mesostructure assembly, which would require larger amphiphilic polymers.[45] Further optimization of non-oxidizing processing methods for particle sintering is also necessary. In this respect, a "brick and mortar" approach which has been used successfully for the preparation of highly crystalline mesoporous titania films[32] could be one of the possibilities to sinter the crystals at lower temperatures and thus to minimize the surface segregation.

CONCLUSIONS

The solvothermal procedure developed in this study enables the preparation of crystalline-doped and undoped nonagglomerated dispersible titania nanoparticles with a narrow particle size distribution and homogeneous incorporation of doping atoms within the host lattice. The particle size and crystallinity can be controlled by the reaction temperature and time. Substitutional doping with niobium ions drastically increases the electrical conductivity of the titania particles. In contrast to the titania particles prepared by a solvothermal synthesis in benzyl alcohol, those of similar size and crystallinity synthesized in *tert*-butyl alcohol can be easily dispersed at high concentrations in THF to form stable colloidal dispersions, which can be attributed to different surface chemistry. The Nb-doped titania nanoparticles can be assembled into regular three-dimensional mesoporous structures with a narrow pore size distribution and high surface area.

EXPERIMENTAL SECTION

All chemicals were purchased from Sigma-Aldrich and used as received. *tert*-Butyl alcohol and benzyl alcohol were dried over 4 Å molecular sieves at 28 °C and filtered prior to use. Pluronic F127 ($EO_{106}PO_{70}EO_{106}$, where EO is ethylene oxide, PO is propylene oxide) was purchased from Sigma-Aldrich.

For the synthesis of niobium-doped titania nanoparticles with different Nb contents, $TiCl_4$ and $Nb(OEt)_5$ were added to *tert*-butyl alcohol (12 mL, 1.8 mmol) under continuous stirring. The particles with different Nb content are designated as NPX, where X is the Nb/(Nb + Ti) molar ratio in percent. As an example for the preparation of NP20 nanoparticles, 0.16 mL (1.44 mmol) of $TiCl_4$ and 0.09 mL (0.36 mmol) of $Nb(OEt)_5$ were used. The clear solution was kept at 100 °C in a laboratory oven in a Teflon-sealed autoclave. The reaction time was 1.5, 3, and 4 h for NP0, NP10, and NP20 nanoparticles, respectively. The onset of the particle formation was determined by evaluating XRD patterns of sample fractions taken from the reaction mixture after different times. The resulting nanoparticles were separated by centrifugation at 50.000 rcf for 15 min. The particles separated this way contain 25−50% of organic residues as determined by thermogravimetric analysis (Netzsch STA 440 C TG/DSC).

For the fabrication of mesostructured films, a solution of Pluronic F127 (0.07 g, 0.006 mmol) in THF (2 mL) was added to 0.2 g of nonwashed particles previously separated by centrifugation (metal oxide content was 1.75 mmol as determined by TGA analysis) and stirred until the particles were homogeneously redispersed. Concentrated HCl (0.2 mL) was added to obtain a clear transparent solution. The mesoporous films were fabricated by dip coating of prepared solutions on various substrates (Si wafer, glass) at a relative humidity of 50−60% and 25 °C. The films were heated in air at 300 °C for 2 h and/or in N_2 at 500 °C for 2 h, with a ramp speed of 0.5 °C min^{-1} for each heating step. The average thickness of the films after heating is around 200 nm.

Wide-angle X-ray diffraction analysis was carried out in reflection mode using a Bruker D8 Discover diffractometer with Ni-filtered Cu Kα radiation (λ = 1.5406 Å) and equipped with a Vantec-1 position-sensitive detector. The crystal lattice *d* spacing and particle size calculations were based on the Bragg equation and Debye−Scherrer equation. The dispersion behavior of nanoparticles was studied by dynamic light scattering using a Malvern Zetasizer-Nano equipped with a 4 mW He−Ne laser (633 nm) and an avalanche photodiode detector.

High-resolution transmission electron microscopy (HRTEM) was performed using a FEI Titan 80-300 instrument equipped with a field emission gun operated at 300 kV. The particulate samples were prepared by evaporating a drop of a diluted suspension of particles in THF on a Plano holey carbon-coated copper grid. HRTEM of films was carried out by removing the thin-film samples from the substrate and transferring them onto a holey carbon-coated copper grid. Scanning electron microscopy (SEM) was performed on a JEOL JSM-6500F scanning electron microscope equipped with a field emission gun at 4 kV.

Small-angle X-ray diffraction was carried out in θ/θ geometry using a Scintag XDS 2000 diffractometer (Scintag Inc.), operated at 40 kV and 30 mA, with Ni-filtered Cu Kα radiation (λ = 1.5406 Å), and a scintillation detector. The textural properties of mesostructured films were analysized with Kr adsorption/desorption measurements at −196 °C using an ASAP 2010 apparatus (Micromeritics).

Electrical conductivity measurements on NTO nanoparticles were performed on pellets prepared by pressing finely ground nanoparticles under a pressure of 10 tons cm^{-2}. To further improve conductivity, thermal treatment under a nitrogen atmosphere was performed at 600 °C for 2 h, with the ramp of 5 °C min^{-1}. The Hall mobility, charge carrier density, and conductivity were measured by the Hall method (ECOPIA HMS 3000) using a magnetic field of 0.55 T.

X-ray photoelectron spectroscopy (XPS) analysis of the particles on a silicon substrate was performed using a VSW HA 100 electron analyzer and the Kα radiation provided by a non-monochromatized magnesium anode system (Mg Kα = 1253.6 eV). Ar ion polishing was performed at 1500 eV. The recorded elemental peaks were fitted by Gaussian−Lorentzian profiles, and the elemental ratios were calculated by the equation

$$\frac{X_A}{X_B} = \frac{I_A/S_A}{I_B/S_B}$$

where I_A/I_B is the ratio of fitted areas, and S is the sensitivity factor.[38]

Supporting Information Available: XRD patterns, XPS spectra, and sizes of Nb−TiO₂ nanoparticles, HRTEM images of mesoporous titania films, XRD patterns of mesostructured Nb−TiO₂ films, and conductivity data of Nb-doped titania nanoparticles. This material is available free of charge *via* the Internet at http://pubs.acs.org.

REFERENCES AND NOTES

1. Fattakhova-Rohlfing, D.; Brezesinski, T.; Rathousky, J.; Feldhoff, A.; Oekermann, T.; Wark, M.; Smarsly, B. Transparent Conducting Films of Indium Tin Oxide with 3D Mesopore Architecture. *Adv. Mater.* **2006**, *18*, 2980–2983.

2. Müller, V.; Rasp, M.; Štefanič, G.; Ba, J.; Günther, S.; Rathouský, J.; Niederberger, M.; Fattakhova-Rohlfing, D. Highly Conducting Nanosized Monodispersed Antimony-Doped Tin Oxide Particles Synthesized via Nonaqueous Sol-Gel Procedure. *Chem. Mater.* **2009**, *21*, 5229–5236.

3. Hou, K.; Puzzo, D.; Helander, M. G.; Lo, S. S.; Bonifacio, L. D.; Wang, W. D.; Lu, Z. H.; Scholes, G. D.; Ozin, G. A. Dye-Anchored Mesoporous Antimony-Doped Tin Oxide Electrochemiluminescence Cell. *Adv. Mater.* **2009**, *21*, 2492–2496.

4. Chopra, K. L.; Major, S.; Pandya, D. K. Transparent Conductors—A Status Review. *Thin Solid Films* **1983**, *102*, 1–46.

5. Wang, Y. D.; Brezesinski, T.; Antonietti, M.; Smarsly, B. Ordered Mesoporous Sb-, Nb-, and Ta-Doped SnO₂ Thin Films with Adjustable Doping Levels and High Electrical Conductivity. *ACS Nano* **2009**, *3*, 1373–1378.

6. Furubayashi, Y.; Hitosugi, T.; Yamamoto, Y.; Inaba, K.; Kinoda, G.; Hirose, Y.; Shimada, T.; Hasegawa, T. A. Transparent Metal: Nb-Doped Anatase TiO₂. *Appl. Phys. Lett.* **2005**, *86*, 252101.

7. Emeline, A. V.; Furubayashi, Y.; Zhang, X. T.; Jin, M.; Murakami, T.; Fujishima, A. Photoelectrochemical Behavior of Nb-Doped TiO₂ Electrodes. *J. Phys. Chem. B* **2005**, *109*, 24441–24444.

8. Hitosugi, T.; Kamisaka, H.; Yamashita, K.; Nogawa, H.; Furubayashi, Y.; Nakao, S.; Yamada, N.; Chikamatsu, A.; Kumigashira, H.; Oshima, M.; *et al.* Electronic Band Structure of Transparent Conductor: Nb-Doped Anatase TiO₂. *Appl. Phys. Expr.* **2008**, *1*, 111203.

9. Lu, X. J.; Mou, X. L.; Wu, J. J.; Zhang, D. W.; Zhang, L. L.; Huang, F. Q.; Xu, F. F.; Huang, S. M. Improved-Performance Dye-Sensitized Solar Cells Using Nb-Doped TiO₂ Electrodes: Efficient Electron Injection and Transfer. *Adv. Funct. Mater.* **2010**, *20*, 509–515.

10. Dros, A. B.; Grosso, D.; Boissiere, C.; Soler-Illia, G. J. d. A. A.; Albouy, P. A.; Amenitsch, H.; Sanchez, C. Niobia-Stabilised Anatase TiO₂ Highly Porous Mesostructured Thin Films. *Microporous Mesoporous Mater.* **2006**, *94*, 208–213.

11. Hirano, M.; Matsushima, K. Photoactive and Adsorptive Niobium-Doped Anatase (TiO₂) Nanoparticles: Influence of Hydrothermal Conditions on Their Morphology, Structure, and Properties. *J. Am. Ceram. Soc.* **2006**, *89*, 110–117.

12. Mattsson, A.; Leideborg, M.; Larsson, K.; Westin, G.; Osterlund, L. Adsorption and Solar Light Decomposition of Acetone on Anatase TiO₂ and Niobium Doped TiO₂ Thin Films. *J. Phys. Chem. B* **2006**, *110*, 1210–1220.

13. Ruiz, A. M.; Dezanneau, G.; Arbiol, J.; Cornet, A.; Morante, J. R. Insights into the Structural and Chemical Modifications of Nb Additive on TiO₂ Nanoparticles. *Chem. Mater.* **2004**, *16*, 862–871.

14. Hasin, P.; Alpuche-Aviles, M. A.; Li, Y.; Wu, Y. Mesoporous Nb-Doped TiO₂ as Pt Support for Counter Electrode in Dye-Sensitized Solar Cells. *J. Phys. Chem. C* **2009**, *113*, 7456–7460.

15. De Koninck, M.; Manseau, P.; Marsan, B. Preparation and Characterization of Nb-Doped TiO₂ Nanoparticles Used as a Conductive Support for Bifunctional CuCo₂O₄ Electrocatalyst. *J. Electroanal. Chem.* **2007**, *611*, 67–79.

16. Furubayashi, Y.; Hitosugi, T.; Yamamoto, Y.; Hirose, Y.; Kinoda, G.; Inaba, K.; Shimada, T.; Hasegawa, T. Novel Transparent Conducting Oxide: Anatase Ti₁₋ₓNbₓO₂. *Thin Solid Films* **2006**, *496*, 157–159.

17. Furubayashi, Y.; Yamada, N.; Hirose, Y.; Yamamoto, Y.; Otani, M.; Hitosugi, T.; Shimada, T.; Hasegawa, T. Transport Properties of d-Electron-Based Transparent Conducting Oxide: Anatase Ti₁₋ₓNbₓO₂. *J. Appl. Phys.* **2007**, *101*, 093705.

18. Haosugi, T.; Ueda, A.; Nakao, S.; Yamada, N.; Furubayashi, Y.; Hirose, Y.; Konuma, S.; Shimada, T.; Hasegawa, T. Transparent Conducting Properties of Anatase Ti₀.₉₄Nb₀.₀₆O₂ Polycrystalline Films on Glass Substrate. *Thin Solid Films* **2008**, *516*, 5750–5753.

19. Hitosugi, T.; Ueda, A.; Furubayashi, Y.; Hirose, Y.; Konuma, S.; Shimada, T.; Hasegawa, T. Fabrication of TiO₂-Based Transparent Conducting Oxide Films on Glass by Pulsed Laser Deposition. *Jpn. J. Appl. Phys. 2* **2007**, *46*, L86–L88.

20. Hitosugi, T.; Ueda, A.; Nakao, S.; Yamada, N.; Furubayashi, Y.; Hirose, Y.; Shimada, T.; Hasegawa, T. Fabrication of Highly Conductive Ti₁₋ₓNbₓO₂ Polycrystalline Films on Glass Substrates *via* Crystallization of Amorphous Phase Grown by Pulsed Laser Deposition. *Appl. Phys. Lett.* **2007**, *90*, 212106.

21. Neumann, B.; Bierau, F.; Johnson, B.; Kaufmann, C. A.; Ellmer, K.; Tributsch, H. Niobium-Doped TiO₂ Films as Window Layer for Chalcopyrite Solar Cells. *Phys. Status Solidi B* **2008**, *245*, 1849–1857.

22. Yamada, N.; Hitosugi, T.; Hoang, N. L. H.; Furubayashi, Y.; Hirose, Y.; Konuma, S.; Shimada, T.; Hasegawa, T. Structural, Electrical and Optical Properties of Sputter-Deposited Nb-Doped TiO₂ (TNO) Polycrystalline Films. *Thin Solid Films* **2008**, *516*, 5754–5757.

23. Zhang, S. X.; Kundaliya, D. C.; Yu, W.; Dhar, S.; Young, S. Y.; Salamanca-Riba, L. G.; Ogale, S. B.; Vispute, R. D.; Venkatesan, T. Niobium Doped TiO₂: Intrinsic Transparent Metallic Anatase *versus* Highly Resistive Rutile Phase. *J. Appl. Phys.* **2007**, *102*, 013701.

24. Zhang, S. X.; Dhar, S.; Yu, W.; Xu, H.; Ogale, S. B.; Venkatesan, T. Growth Parameter-Property Phase Diagram for Pulsed Laser Deposited Transparent Oxide Conductor Anatase Nb: TiO₂. *Appl. Phys. Lett.* **2007**, *91*, 112113.

25. Noh, J. H.; Lee, S.; Kim, J. Y.; Lee, J. K.; Han, H. S.; Cho, C. M.; Cho, I. S.; Jung, H. S.; Hong, K. S. Functional Multilayered Transparent Conducting Oxide Thin Films for Photovoltaic Devices. *J. Phys. Chem. C* **2009**, *113*, 1083–1087.

26. Morris, D.; Dou, Y.; Rebane, J.; Mitchell, C. E. J.; Egdell, R. G.; Law, D. S. L.; Vittadini, A.; Casarin, M. Photoemission and STM Study of the Electronic Structure of Nb-Doped TiO₂. *Phys. Rev. B* **2000**, *61*, 13445–13457.

27. Sheppard, L.; Bak, T.; Nowotny, J.; Sorrell, C. C.; Kumar, S.; Gerson, A. R.; Barnes, M. C.; Ball, C. Effect of Niobium on the Structure of Titanium Dioxide Thin Films. *Thin Solid Films* **2006**, *510*, 119–124.

28. Sheppard, L. R.; Bak, T.; Nowotny, J. Electrical Properties of Niobium-Doped Titanium Dioxide. 1. Defect Disorder. *J. Phys. Chem. B* **2006**, *110*, 22447–22454.

29. Sheppard, L. R.; Bak, T.; Nowotny, J. Electrical Properties of Niobium-Doped Titanium Dioxide. 2. Equilibration Kinetics. *J. Phys. Chem. B* **2006**, *110*, 22455–22461.

30. Grosso, D.; Soler-Illia, G. J. d. A. A.; Babonneau, F.; Sanchez, C.; Albouy, P. A.; Brunet-Bruneau, A.; Balkenende, A. R. Highly Organized Mesoporous Titania Thin Films Showing Mono-oriented 2D Hexagonal Channels. *Adv. Mater.* **2001**, *13*, 1085–1090.

31. Hwang, Y. K.; Lee, K. C.; Kwon, Y. U. Nanoparticle Routes to Mesoporous Titania Thin Films. *Chem. Commun.* **2001**, 1738–1739.

32. Szeifert, J. M.; Fattakhova-Rohlfing, D.; Georgiadou, D.; Kalousek, V.; Rathousky, J.; Kuang, D.; Wenger, S.; Zakeeruddin, S. M.; Grätzel, M.; Bein, T. "Brick and Mortar" Strategy for the Formation of Highly Crystalline Mesoporous Titania Films from Nanocrystalline Building Blocks. *Chem. Mater.* **2009**, *21*, 1260–1265.

33. Müller, V.; Rasp, M.; Rathouský, J.; Schütz, B.; Niederberger, M.; Fattakhova-Rohlfing, D. Transparent Conducting Films of Antimony-Doped Tin Oxide with Uniform Mesostructure Assembled from Preformed Nanocrystals. *Small* **2010**, *6*, 633–637.

34. Szeifert, J. M.; Feckl, J. M.; Fattakhova-Rohlfing, D.; Liu, Y.; Kalousek, V.; Rathousky, J.; Bein, T. Ultrasmall Titania Nanocrystals and Their Direct Assembly into Mesoporous Structures Showing fast Lithium Insertion. *J. Am. Chem. Soc.* DOI: 10.1021/ja101810e.

35. Arbiol, J.; Cerda, J.; Dezanneau, G.; Cirera, A.; Peiro, F.; Cornet, A.; Morante, J. R. Effects of Nb Doping on the TiO_2 Anatase-to-Rutile Phase Transition. *J. Appl. Phys.* **2002**, *92*, 853–861.

36. Di Valentin, C.; Pacchioni, G.; Selloni, A. Reduced and n-Type Doped TiO_2: Nature of Ti^{3+} Species. *J. Phys. Chem. C* **2009**, *113*, 20543–20552.

37. Atashbar, M. Z.; Sun, H. T.; Gong, B.; Wlodarski, W.; Lamb, R. XPS Study of Nb-Doped Oxygen Sensing TiO_2 Thin Films Prepared by Sol−Gel Method. *Thin Solid Films* **1998**, *326*, 238–244.

38. Dacca, A.; Gemme, G.; Mattera, L.; Parodi, R. XPS Analysis of the Surface Composition of Niobium for Superconducting RF Cavities. *Appl. Surf. Sci.* **1998**, *126*, 219–230.

39. Kubacka, A.; Colon, G.; Fernandez-Garcia, M. Cationic (V, Mo, Nb, W) Doping of TiO_2-Anatase: A Real Alternative for Visible Light-Driven Photocatalysts. *Catal. Today* **2009**, *143*, 286–292.

40. Hitosugi, T.; Kinoda, G.; Yamamoto, Y.; Furubayashi, Y.; Inaba, K.; Hirose, Y.; Nakajima, K.; Chikyow, T.; Shimada, T.; Hasegawa, T. Carrier Induced Ferromagnetism in Nb Doped Co: TiO_2 and Fe: TiO_2 Epitaxial Thin Film. *J. Appl. Phys.* **2006**, *99*, 08M121.

41. Niederberger, M. Nonaqueous Sol−Gel Routes to Metal Oxide Nanoparticles. *Acc. Chem. Res.* **2007**, *40*, 793–800.

42. Zunger, A. Practical Doping Principles. *Appl. Phys. Lett.* **2003**, *83*, 57–59.

43. Norris, D. J.; Efros, A. L.; Erwin, S. C. Doped Nanocrystals. *Science* **2008**, *319*, 1776–1779.

44. Mikulec, F. V.; Kuno, M.; Bennati, M.; Hall, D. A.; Griffin, R. G.; Bawendi, M. G. Organometallic Synthesis and Spectroscopic Characterization of Manganese-Doped CdSe Nanocrystals. *J. Am. Chem. Soc.* **2000**, *122*, 2532–2540.

45. Grosso, D.; Boissiere, C.; Smarsly, B.; Brezesinski, T.; Pinna, N.; Albouy, P. A.; Amenitsch, H.; Antonietti, M.; Sanchez, C. Periodically Ordered Nanoscale Islands and Mesoporous Films Composed of Nanocrystalline Multimetallic Oxides. *Nat. Mater.* **2004**, *3*, 787–792.